Geophysical Research Letters

Variable Basal Melt Rates of Antarctic Peninsula Ice Shelves, 1994–2016

Susheel Adusumilli[1] (iD), **Helen Amanda Fricker[1]**, **Matthew R. Siegfried[1,2]** (iD), **Laurie Padman[3]** (iD), **Fernando S. Paolo[1,4]**, and **Stefan R. M. Ligtenberg[5]** (iD)

[1]Scripps Institution of Oceanography, University of California, San Diego, La Jolla, CA, USA, [2]Department of Geophysics, Stanford University, Palo Alto, CA, USA, [3]Earth and Space Research, Corvallis, OR, USA, [4]Jet Propulsion Laboratory, California Institute of Technology, Pasadena, CA, USA, [5]Institute for Marine and Atmospheric Research Utrecht, Utrecht University, Utrecht, Netherlands

Abstract We have constructed 23-year (1994–2016) time series of Antarctic Peninsula (AP) ice-shelf height change using data from four satellite radar altimeters (ERS-1, ERS-2, Envisat, and CryoSat-2). Combining these time series with output from atmospheric and firn models, we partitioned the total height-change signal into contributions from varying surface mass balance, firn state, ice dynamics, and basal mass balance. On the Bellingshausen coast of the AP, ice shelves lost 84 ± 34 Gt a^{-1} to basal melting, compared to contributions of 50 ± 7 Gt a^{-1} from surface mass balance and ice dynamics. Net basal melting on the Weddell coast was 51 ± 71 Gt a^{-1}. Recent changes in ice-shelf height include increases over major AP ice shelves driven by changes in firn state. Basal melt rates near Bawden Ice Rise, a major pinning point of Larsen C Ice Shelf, showed large increases, potentially leading to substantial loss of buttressing if sustained.

Plain Language Summary Antarctica's ice shelves regulate the flow of grounded ice into the ocean, and enhancing our processes that control how ice shelves respond to atmospheric and oceanic drivers will ultimately improve estimates of sea level change. We have generated a 23-year record of ice-shelf height changes for the Antarctic Peninsula region using four satellite altimeters. We focussed our analysis on the height variability rather than just the long-term trends so that we can better separate the contributions of the ocean and the atmosphere. Most ice shelves on the Peninsula showed height increases since 2009, at least temporarily reversing previously reported trends of declining height. At Larsen C Ice Shelf on the eastern coast of the Peninsula, this reversal was caused by reduced summertime surface melting. The resulting increase in surface-snow air content may reduce the susceptibility of this ice shelf to the surface-melt-driven collapse previously seen on nearby ice shelves. We also found large variations in how fast the ocean is eroding the base of this ice shelf near a pinning point crucial to its stability. On the western coast, while their surface heights have also recently increased, the ice shelves have continued to lose mass from excess ocean melting.

1. Introduction

Ice shelves around the periphery of Antarctica connect the grounded ice sheet to the Southern Ocean and are influenced by changes in the ocean, atmosphere, and ice sheet dynamics. Confined ice shelves exert back-stresses on grounded ice, a process called buttressing (Dupont & Alley, 2005). When buttressing is reduced through ice-shelf collapse, substantial thinning, or mechanical weakening of the shear margins, ice streams and outlet glaciers that flow into it accelerate (e.g., Pritchard et al., 2012; Rignot et al., 2004; Scambos et al., 2004), contributing to sea level rise.

The Antarctic Peninsula (AP; Figure 1), the northernmost region of Antarctica, has experienced dramatic reductions in ice-shelf extent (Cook & Vaughan, 2010) and surface height (Paolo, Fricker, & Padman, 2015) in the last few decades. On the eastern (Weddell Sea) side, the collapses of Prince Gustav and Larsen A ice shelves in 1995 were followed by the rapid collapse of most of Larsen B Ice Shelf (LBIS) in 2002. On the western (Bellingshausen Sea) side, the small Müller, Jones, and Wordie ice shelves have all collapsed or substantially retreated, and Wilkins Ice Shelf (WIS) lost a significant portion of its area during large break-up events in 2008 and 2009 (Cook & Vaughan, 2010). Most remaining AP ice shelves have experienced changes in surface height, as measured by satellite altimeters (Fricker & Padman, 2012; Paolo, Fricker, & Padman, 2015; Pritchard et al., 2012), with an overall surface lowering during the time periods covered by these studies.
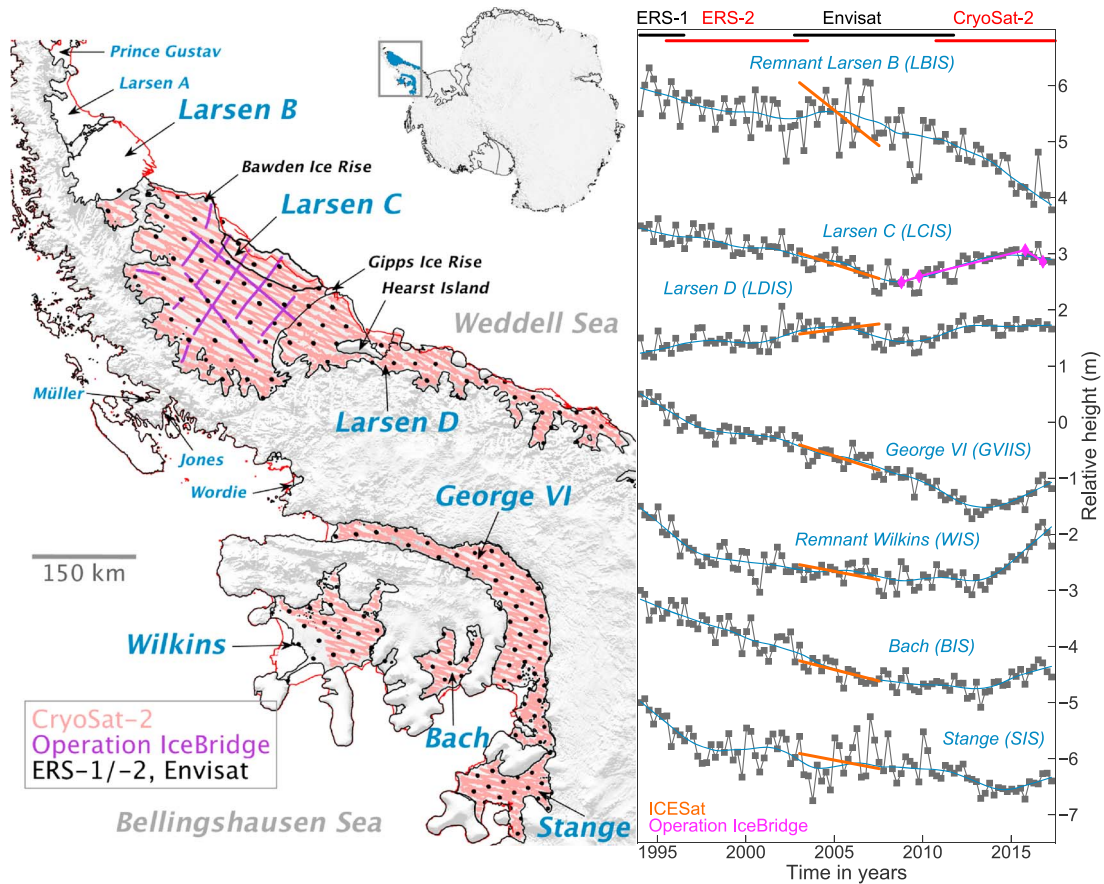
Figure 1. (left) Map of Antarctic Peninsula showing locations of radar and laser altimeter data used in this study: ground tracks for three months of CryoSat-2 (red lines), crossovers for three months of the 35-day repeat orbit of ERS-1 (Phases C and G), ERS-2, and Envisat (black dots), and NASA's Operation IceBridge flights flown in 2008, 2009, 2015, and 2016 (purple lines). Black line on Larsen C Ice Shelf shows outline of iceberg A-68 (A. Luckman, personal communication, 2017), which calved in July 2017. Red outlines show ice-shelf extent in the late 1980s (Cook & Vaughan, 2010). Background image is from the MODIS Mosaic of Antarctica (Scambos et al., 2007). (right) Ice-shelf averaged height changes over Antarctic Peninsula ice shelves, 1994–2017. Black squares show three-month averages; blue lines are three-year filtered heights; red lines are 2003–2008 height-change estimates from ICESat laser altimetry (Pritchard et al., 2012); purple lines on the Larsen C Ice Shelf time series are height-change time series from IceBridge airborne laser altimetry.

Declining extent and height of AP ice shelves have been attributed to a complex set of processes involving the atmosphere, ocean, and sea ice. Morris and Vaughan (2003) noted that the timing and location of major collapse events coincided with the southward migration of the mean-annual −9°C isotherm driven by regional atmospheric warming during the last half of the twentieth century; this isotherm was used as a proxy for summer surface melting that can lead to hydrofracture (Scambos et al., 2000; van den Broeke, 2005). Direct atmospheric controls on ice-shelf height include variability of surface mass balance (SMB) (e.g., Kuipers Munneke et al., 2017), density of near-surface firn (Pritchard et al., 2012), and atmospheric pressure inducing changes in ocean surface height (Padman et al., 2003). Atmospheric changes are a combination of natural variability whose role in Antarctic atmospheric state is still poorly understood (Turner et al., 2016), and anthropogenic effects including increased global greenhouse gas concentrations and changing stratospheric ozone levels (Arblaster & Meehl, 2006; Thompson & Solomon, 2002). Changes in atmospheric conditions, notably wind stress, on a wide range of scales from local to global, also alter circulation of subsurface warm water on continental shelves, which in turn drives variations in ice-shelf basal mass balance (BMB) (e.g., Dutrieux et al., 2014; Holland, Jenkins, & Holland, 2010; Paolo et al., 2018). Wind-driven changes in sea-ice concentration and thickness also alter the effect of wind stress on ocean circulation (Kim et al., 2017), ocean-atmosphere heat exchange and ocean mixing (Dinniman et al., 2012), and the production rate of deep water in coastal polynyas, which can modify ocean heat flux under ice shelves (Khazendar et al., 2013).

2. Previous AP Satellite Altimeter Studies

Shepherd et al. (2003) reported net surface lowering of Larsen C Ice Shelf (LCIS; see Figure 1 for location) based on satellite radar altimetry (RA) for the period 1992–2001 and attributed this lowering to basal melting in excess of the rate required for steady-state mass balance. Fricker and Padman (2012) used height differences at crossover locations between ground tracks of Seasat RA (July to October 1978) and the beginning of the ERS-1 mission (June to October 1992) to show that this surface lowering started before 1992. Pritchard et al. (2012) showed that patterns and magnitudes of time-averaged LCIS height changes derived from ICESat satellite laser altimetry from 2003 to 2008 were consistent with modeled height change from SMB and firn processes, meaning that the basal melt rate during this period was consistent with the value required for steady-state ice-shelf mass balance.

On the Bellingshausen coast, time series of inferred ice thickness (*H*) for individual ice shelves show substantial temporal variability in *dH/dt* (Paolo et al., 2015; see their Figure S1A). In particular, WIS and Stange Ice Shelf (SIS) thinned rapidly from 1994 to 2000, then remained fairly stable until 2012 (the end of the record). George VI Ice Shelf (GVIIS) showed high thinning rates throughout the period 1994–2012.

Padman et al. (2012) reported that *dH/dt* for WIS switched in the year 2000 from a steady decline to approximately steady state, consistent with a rapid reduction in inferred basal melt rate. They attributed the change in melt rate to retreat of the ice base upward from the thick benthic layer of warm Circumpolar Deep Water (CDW) into the cold, fresh upper layer of Winter Water. Continued melting of GVIIS throughout this period is consistent with its ice draft being much deeper than that of WIS (Figure 2a), so that its base remained in the warmer CDW layer.

3. Deriving Height Changes and Basal Melt Rates

We used RA data from the CryoSat-2 mission (Wingham et al., 2006) to extend the existing 18-year (1994–2012) ice-shelf height-change records developed by Paolo et al. (2015, 2016) to mid-2017, resulting in a continuous 23-year record of the changes in surface height, *h(t)*, sampled every three months. For consistency with Paolo et al. (2015, 2016), we averaged CryoSat-2 values of *h(t)* in grid cells of 0.25° in latitude and 0.75° in longitude (~30 × 30 km) and three-month time steps (see the supporting information). We excluded all RA data less than 3 km from the grounding line; this minimized contamination from the flexural boundary layer near the grounding zone where the ice is not fully hydrostatic and tide-model corrections are not valid.

The rate of change of *h* is a combination of several processes represented by

$$\frac{dh}{dt} = \frac{(\rho_w - \rho_i)}{\rho_w}\left(\frac{M_s}{\rho_i} - \nabla \cdot (\overline{v}H) - w_b\right) + \frac{dh_s}{dt},$$ (1)

where ρ_w and ρ_i are the densities of seawater ($1{,}028 \pm 1$ kg m^{-3}) and ice (917 ± 5 kg m^{-3}); $\nabla\cdot(\overline{v}H)$ (m a^{-1}) is the sum of ice advection ($\overline{v}\cdot\nabla H$) and divergence ($H\nabla\cdot\overline{v}$), with $\overline{v}$ being ice velocity and *H* ice-shelf thickness in meters of solid-ice equivalent; M_s (kg · m^{-2} · a^{-1}) is the SMB; w_b (m a^{-1}) is the basal melt rate in meters of solid-ice equivalent per year (negative for marine-ice growth); and h_s (m) is the contribution to buoyancy-corrected height from changes in density in the firn column. We obtained maps of $\overline{v}$ from Mouginot et al. (2017) and *H* from ice thicknesses derived from CryoSat-2 RA referenced to velocity acquisition times (see the supporting information). We obtained M_s from a regional atmospheric model (RACMO version 2.3p2; Van Wessem et al., 2017), and estimated dh_s/dt from a firn densification model (IMAU-FDM; Ligtenberg et al., 2011) driven by RACMO2.3p2 output, both at 5.5 km horizontal spacing (Van Wessem et al., 2016). Using equation (1), we then derived w_b as the residual of all other terms. At the time of writing, the IMAU-FDM simulation extends only to the end of 2016; therefore, all quantities that depend on this model are for the period 1994–2016 inclusive (i.e., 23 years). All uncertainties presented in this paper are 95% confidence intervals (unless stated otherwise). We assume that SMB and firn model outputs have correlated errors within individual ice shelves, resulting in conservative error estimates for our ice-shelf averaged values.
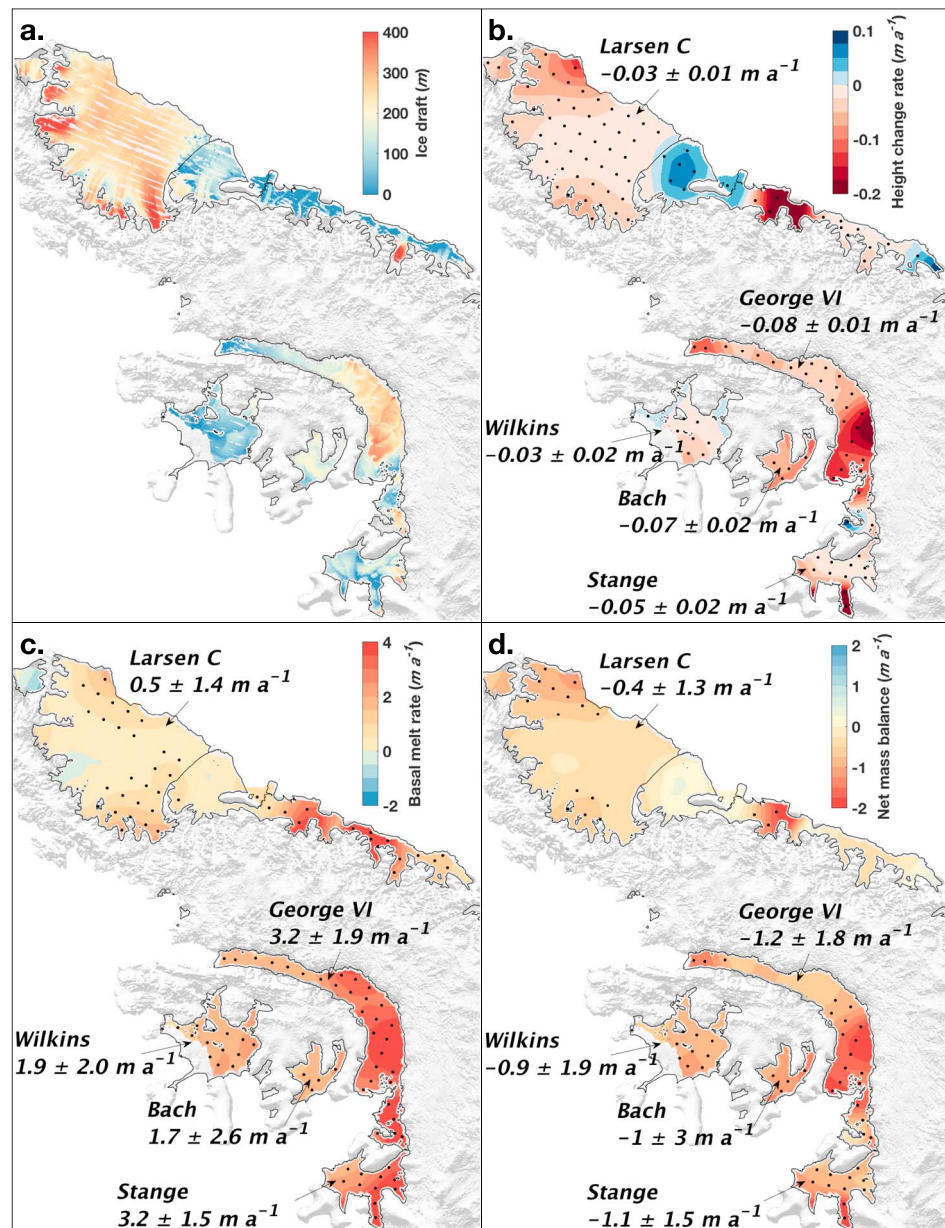
Figure 2. (a) Ice draft from CryoSat-2 RA at 2 km resolution (see the supporting information). Mean values of (b) height-change rates (dh/dt), (c) basal melt rates (w_b), and (d) net mass balance for the period 1994–2016 over Antarctic Peninsula ice shelves. Stippling indicates locations of grid cells with rates above the 67% confidence interval.

4. Results and Discussion

4.1. Surface Height Time Series, Trends, and Basal Melt Rates

Most regions of AP ice shelves experienced overall surface lowering between 1994 and 2016 (Figures 1 and 2b), with rates exceeding -0.3 m a^{-1} on portions of northern LCIS, southern GVIIS, and SIS. Surface height for the northern portion of Larsen D Ice Shelf (LDIS) increased over the 23-year period (Figure 2b).

The map of the 23-year averaged basal melt rate w_b (Figure 2c), derived from equation (1), shows that the highest melt rates occur under the southern GVIIS and portions of SIS and LDIS. The ice-shelf averaged estimates of w_b likely underestimate the true values because of our exclusion of all RA data less than 3 km from the grounding line; these data are from regions of thick ice in the grounding zone, where melt rates are expected to be relatively high (Jenkins, 2011). Another potential bias is inherent to the IMAU-FDM, which

requires that the net firn-height change from the beginning (1979) to the end (2016) of the simulation be zero due to the steady-state assumption made to obtain a realistic initial firn column (Ligtenberg et al., 2011). This constraint implies a zero-mean value of dh_s/dt between 1979 and 2016 (Figure S1). Over the AP ice shelves, this assumption can contribute uncertainties from ±0.8 to ±2.4 m a^{-1} in the steady state w_b estimates in individual grid cells, as derived using sensitivity tests described by Pritchard et al. (2012). The magnitude of this error over any individual grid cell primarily depends on the uncertainty in the height change due to surface melting.

In the following two sections, we summarize the observed temporal variability for the major AP ice shelves and discuss relationships between this variability and forcing by the atmosphere and ocean.

4.2. Weddell Coast Ice Shelves

The Weddell coast of the AP is currently occupied by three ice shelves: the remnant portion of LBIS, the large LCIS, and the generally narrow LDIS. The remnant LBIS was sampled by only two ground-track crossover locations of the ERS and Envisat orbits on the freely floating ice shelf (Figure 1). There was a decrease in height at these crossover locations prior to the 2002 collapse of LBIS, followed by a short period of height increase from 2002 to 2005, and then a return to surface lowering (Figure 1). However, because of the poor sampling, we limit discussion of remnant LBIS mass balance. The broad region of northern LDIS, south of Gipps Ice Rise but north of Hearst Island, is reasonably well sampled (Figure 1), but the southern portion consists of a series of narrow, floating ice tongues with high topographic gradients, which results in a lower signal-to-noise ratio in the RA data.

The 23-year net mass balance for LCIS shows mass loss in key regions such as near Bawden Ice Rise (BIR) and the southern grounding line (Figure 2d). The ice-shelf averaged mean w_b is 0.5 ± 1.4 m a^{-1} (Table S1). This low value of w_b is consistent with ocean measurements obtained in February 2002 offshore of the northern LCIS ice front (Nicholls et al., 2004). This study showed that the subsurface layer of Ice Shelf Water flowing out of the ocean cavity beneath LCIS was sourced from cold, saline, Modified Weddell Deep Water (MWDW, with temperature $T_{ocean} < -1.5°C$) that must have been cooled to near the surface freezing point ($T_{ocean} \approx -1.9°C$) before coming into contact with the LCIS base. This cold water would not contain sufficient heat to cause substantial basal melting beyond the point of initial contact with thick ice at the grounding line (Jenkins, 2011).

The LCIS height record for 1994–2017 (Figure 1) shows substantial multiannual variability, with a cumulative surface lowering of 1.0 ± 0.3 m from 1994 to 2009 followed by a surface rising of 0.5 ± 0.3 m from 2009 to 2017. This recent surface rising of LCIS, largely occurring on the northern portion of the ice shelf (Figures 3d and 3e), is a previously undocumented change in the long-term behavior of LCIS. We considered the possibility that the height increase detected by RA may have been related to an upward migration of the radar-reflection horizon within the snowpack, as observed in Greenland (e.g., Nilsson et al., 2015; Thomas et al., 2008). To test this hypothesis, we derived an independent time series of height change on LCIS from Operation IceBridge (OIB) laser altimetry data acquired during the austral summers of 2009, 2010, 2015, and 2016. Unlike microwave-band radar, OIB's visible-band laser reflects from the top surface of the snow or firn and thus can be used to distinguish between a vertically moving internal reflector and true surface-height changes. The OIB-derived height changes were consistent, within measurement uncertainty, with the RA-derived height changes (Figure 1), and so we conclude that a rising internal radar-reflection horizon is unlikely to be the cause of the RA-derived height change in this case. Recent (2011 to 2016) RA-derived changes approximately correspond with variability in the IMAU-FDM simulated time series of h_s (Figures 3f–3j and S2), suggesting that increasing firn-air content is the primary contributor to LCIS height increase in this period.

Changes in h_s over LCIS are significantly influenced by surface melting (Pritchard et al., 2012), which occurs primarily during austral summers (December to February; see Figure S1). During summers with anomalously low temperatures, surface melting is reduced, causing a smaller decrease in firn-air content through time than in an average summer; this would lead to a relative increase in h_s. The six-year averaged summer temperature anomalies (relative to the 1979–2016 mean) over LCIS were lower for the 2011–2016 epoch than for any other six-year epoch since 1995 (Figures 3k–3o), as were surface melt anomalies (Figures S2a–S2e). Similar decadal behavior is not apparent in snowfall (Figures S2f–S2j). An increase in air content, as observed over LCIS between 2011 and 2015, could allow more meltwater storage in existing pore space,
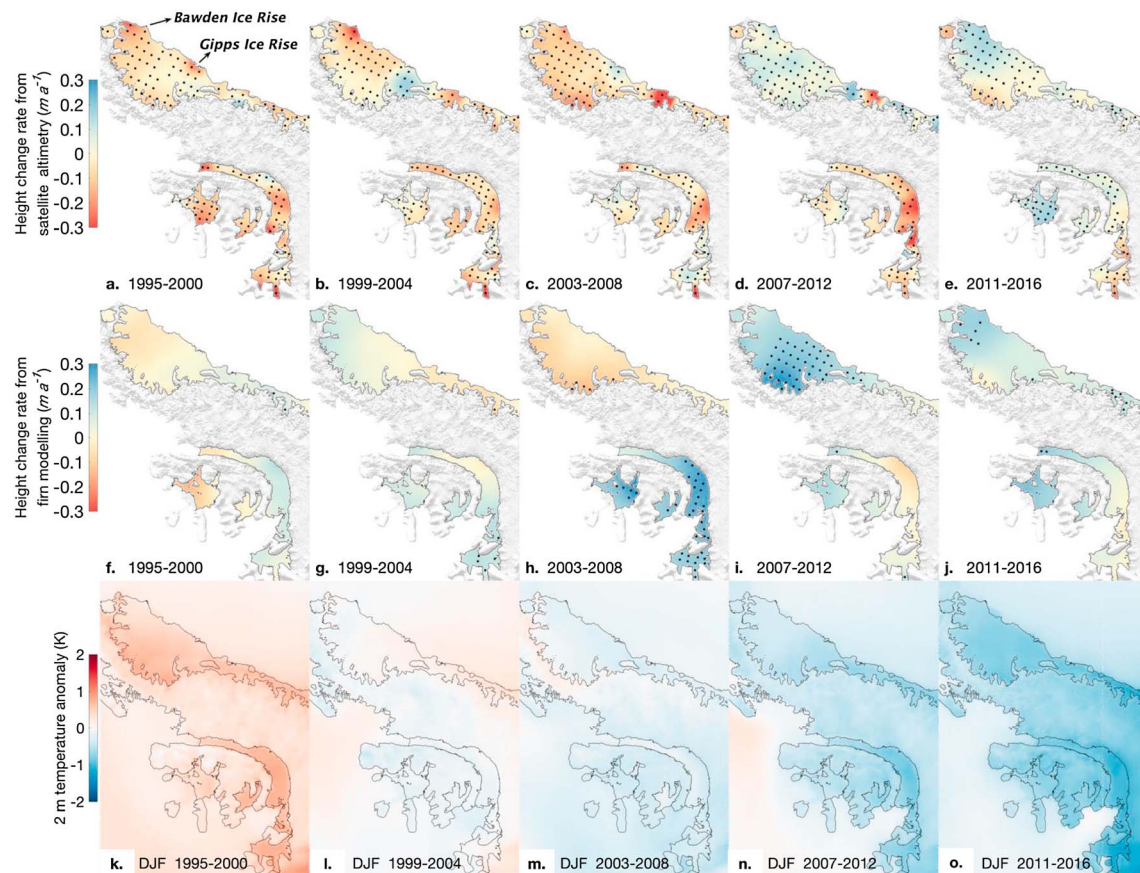
Figure 3. Spatial patterns of ice-shelf height changes for five overlapping six-year epochs between 1995 and 2016, from (a–e) satellite radar altimetry and (f–j) the IMAU-FDM firn model. Stippling indicates locations of grid cells with height change rates above their 67% confidence interval. (k–o) Austral summer (December-January-February; DJF) temperature anomalies at 2 m height, relative to the 1979–2016 mean values from the regional atmospheric model RACMO2.3p2.

reducing susceptibility to hydrofracture that can occur when melt ponds form on the surface in summer (Scambos et al., 2013).

On multiannual time scales, the largest height-change rate observed on LCIS was in the north during 1999–2008 (Figures 3b and 3c), corresponding to high w_b anomalies (Figure 4a). Near BIR, height decreased at a rate of -0.27 ± 0.08 m a^{-1} during this period (Figure 4b), averaged over the ~512 km^2 of ice shelf within the grid cell containing BIR. We estimated the time series of various components of mass balance in this region (Figure S3). Time series of w_b was temporally variable, with a maximum of 5 ± 2 m a^{-1} in 2002 (Figure 4c). Since BIR is a significant pinning point for LCIS, basal melting at this rapid rate, if sustained, would lead to reduced contact of the ice shelf with the bed and decrease the stability of LCIS (Borstad et al., 2013, 2017; Holland et al., 2015).

The spatial pattern of the melt rate anomaly for the period 1999–2008 for LCIS and northern LDIS (Figure 4a) is qualitatively similar to the map of modeled w_b reported by Mueller et al. (2012) for a tide-forced simulation with cold water (T_{ocean} of -1.9 to -1.7°C) entering the sub–ice-shelf cavity (their Figure 8). The higher melt rates around BIR during an approximately four-year period centered on 2002 (Figure 4c) are consistent with an increase in ocean temperature around BIR during this period; the model by Mueller et al. (2012) suggests that an increase in T_{ocean} of ~0.2°C would explain the increase in w_b in this region where mixing is dominated by tidal currents. This warmer water (MWDW), with $T_{ocean} \sim -1.7$°C, has been observed just offshore of the LCIS ice front (Nicholls et al., 2004). Our observations, combined with the Mueller et al. (2012) model, suggest that the period of increased w_b may be caused by local inflow of MWDW across the northern LCIS ice front. In this scenario, the subsurface layer of Ice Shelf Water observed by Nicholls et al. (2004) in February 2002 (near
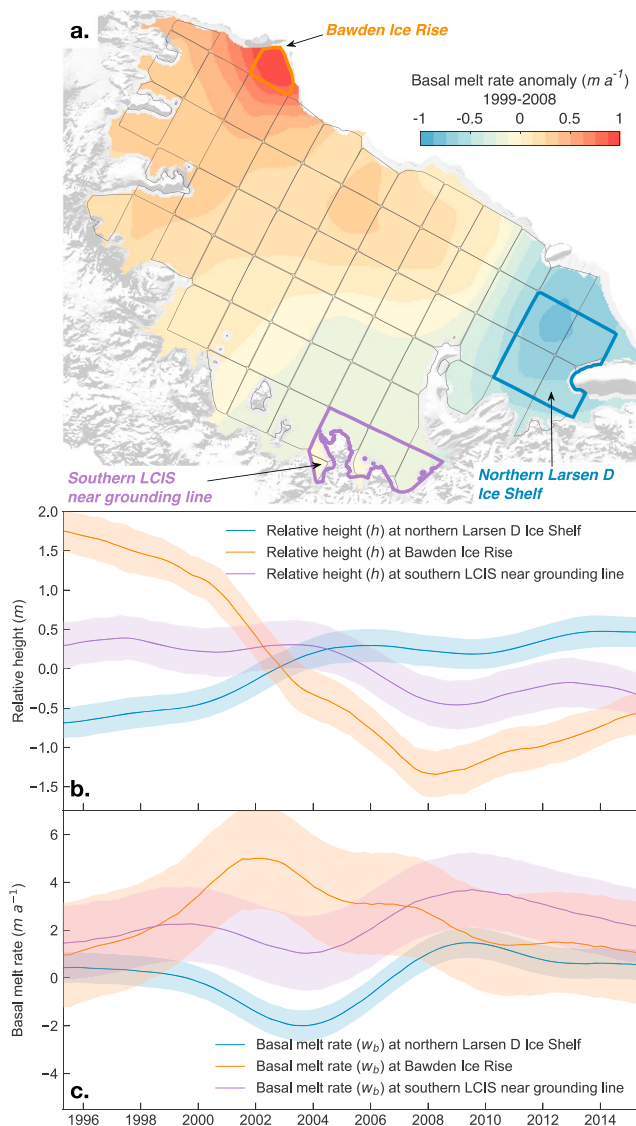
Figure 4. Spatial and temporal variabilities of basal melt rates for Larsen C and northern Larsen D ice shelves. (a) Average basal melt rate (m a^{-1}) for the period 1999–2008, relative to the average for 1994–2016. Time series of spatially averaged (b) heights and (c) basal melt rates for regions identified on the map by colored outlines: Bawden Ice Rise (orange), northern Larsen D Ice Shelf (blue), and near the southern Larsen C Ice Shelf grounding line (purple).

the time of maximum w_b around BIR) would represent a meltwater plume from deeper under LCIS where the initial source of heat to the ice is High Salinity Shelf Water ($T_{ocean} \sim -1.9°C$), while the region around BIR melted rapidly as the tidal currents mixed relatively warm MWDW ($T_{ocean} \sim -1.7°C$) to the ice base.

The 1999–2008 basal melt rate anomaly around BIR was of opposite sign to the anomalies near the deep grounding lines of the southern part of LCIS and northern LDIS (Figures 4a and 4c). We hypothesize that the approximately four-year period with high w_b around BIR corresponds to a time when relatively warm water from outside the cavity could reach the ice base around BIR because of a reduction in the flux of cold meltwater from southern LCIS and northern LDIS; see a related study of Filchner-Ronne Ice Shelf by Mueller et al. (2018).

4.3. Bellingshausen Coast Ice Shelves

Most large ice shelves along the Bellingshausen coast showed net surface lowering from 1994 to 2017 (Figure 2b). In general, the lowest heights were recorded near 2013, after which heights increased until 2016 (Figure 1). The average net mass balance was -1.2 ± 1.8 m a^{-1}, arising from a basal melt rate of 3.2 ± 1.9 m a^{-1}, compared with the value of 2.0 ± 0.4 m a^{-1} required to balance the sum of SMB and $\nabla \cdot (\overline{v}H)$ (Table S1). These basal melt rates, which are large relative to those for LCIS, are consistent with ocean observations showing the presence of warm CDW, with temperature above 0°C, near the two ice fronts of GVIIS (Jenkins & Jacobs, 2008) and beneath GVIIS (Potter & Paren, 1985). Basal melt rates were highest, up to 7 ± 2 m a^{-1} in the southern portion of GVIIS (Figure 2c) where the ice draft is deeper (Figure 2a). A measured increase in outlet-glacier velocities from 1992 to 2015 in this region (Hogg et al., 2017) is consistent with sustained ice-shelf mass loss (Figure 2d) reducing buttressing of the adjacent grounded ice.

The remnant portion of WIS has experienced height changes on multiannual timescales (Figure 1), with a surface lowering of 1.1 ± 0.1 m from 1994 to 1998 followed by a period of reduced net lowering of 0.4 ± 0.1 m between 1998 and 2013, and then a more recent height increase of 1.2 ± 0.1 m. The rapid increase in surface height since 2013 recovered most of the height that was lost prior to 2013. Differences between trends in height (Figure 2b) and mass (Figure 2d) can be attributed to the contribution to height change from changes in the firn column (Figure S1).

The recent increases in surface heights of SIS, Bach Ice Shelf, and WIS appear to be mainly related to surface accumulation changes and firn variability (Figure S1). Spatial variability in basal melt rates between the Bellingshausen coast ice shelves is likely related to differences in ocean circulation. The relatively shallow ice drafts of SIS, Bach Ice Shelf, and WIS ice shelves (Figure 2a), compared with that of GVIIS, make them more susceptible to upper-ocean processes that can change on seasonal scales, with a potentially strong dependence on coastal atmospheric conditions (Padman et al., 2012).

5. Conclusions

We have used multimission satellite RA to construct time series of ice-shelf surface height change h(t) across the AP. We used h(t) records, ice velocity data, and regional atmospheric and firn modeling to estimate the various components of ice shelf mass balance between 1994 and 2016. Overall, the 23-year mean basal melt rates across the AP exceeded those required to balance mean SMB, ice advection, and ice divergence, leading to net ice mass loss. The highest excess melt rates (~1 m a^{-1} ice equivalent) occurred on the Bellingshausen

coast, which we attribute to enhanced inflow of warm CDW ($T > 0$°C) under the ice shelves. In the Weddell Sea, where water temperatures on the continental shelf are cold, and constrained to a narrow range (about -1.9 to -1.7°C) (e.g., Pritchard et al., 2012; Schmidtko et al., 2014), the time-averaged excess basal melt rate under LCIS was ~0.4 m a^{-1}.

On shorter time scales, however, most variability in height change was driven by changes in firn height (Figure S2). The largest contribution to height change from modeled firn variability occured on the Bellingshausen coast ice shelves, with firn height changing up to 2.5 m during the period 1994–2016. On LCIS, firn height changed up to ~1.3 m within the same period, which caused significant variations in measured h including a previously undocumented sustained increase in ice-shelf surface height after 2009. This latter period coincided with cooler summer air temperatures, which we expect would reduce the magnitude of annual firn densification due to surface melting.

Changes in height and mass of AP ice shelves have implications both for their stability and for the adjacent grounded ice. On the Bellingshausen side of the AP, mass loss from GVIIS, especially in its southern portion, appears to have produced a dynamic grounded-ice response: glaciers feeding this ice shelf have accelerated (Hogg et al., 2017; Minchew et al., 2018). On the eastern side, the basal melt rate on LCIS near BIR, an important pinning point for LCIS, can vary from negligible to 5 ± 2 m a^{-1}. If enhanced melt rates were sustained for several years, buttressing of LCIS by BIR could be substantially reduced. Given that melt rates around BIR are expected to depend primarily on ocean temperature (Mueller et al., 2012), future changes in buttressing of LCIS by BIR will depend on the changing contributions of ocean heat supply from MWDW and High Salinity Shelf Water flowing under the northern ice front, as well as cold meltwater plumes flowing from deeper under LCIS.

Previous satellite radar altimeter studies have generally only reported straight-line trends over short, single-mission observation periods. Our record, however, is sufficiently long to link ice-shelf variability to (specific?) amospheric and oceanic processes. While we have speculated on the contributions of such processes toward the variability in our derived time series, there are insufficient ocean data from near any of the major AP ice shelves to confirm the inferred relationships between ocean state and ice-shelf response. However, we expect that our new data set for basal mass balance terms will be valuable for testing current and future numerical models of ice-shelf response to climate variability in this region. Our study demonstrates the need for ongoing continuous monitoring of Antarctic ice shelves by satellite altimetry, and the importance of generating long, accurate time series so that we can fully understand the mechanisms involved in ice-shelf-ocean interaction, which will eventually enable us to confidently include this behavior in ice sheet models.

Data Availability

ERS-1, ERS-2, Envisat, and CryoSat-2 radar altimetry data are available from the European Space Agency (ERS-1 and ERS-2 data from ftp://ra-ftp-ds.eo.esa.int/, Envisat data from ftp://ra2-ftp-ds.eo.esa.int/, and CryoSat-2 level-2 SARIn-mode data from ftp://science-pds.cryosat.esa.int/SIR_SIN_L2). Processed height-change time series constructed from all four radar altimeters (1994-2017) over the AP are an update to Paolo et al. (2015, 2016) for this region and available on NASA's sea level rise data portal at https://sealevel.nasa.gov/data/dataset/?identifier=SLCP_AP_iceshelf_heights_1. The various derived components of steady state ice-shelf mass balance between 1994 and 2016, including time-variable basal melt rates for Larsen C and northern Larsen D ice shelves, are at https://sealevel.nasa.gov/data/dataset/?identifier=SLCP_AP_iceshelf_mass_balance_1. Airborne laser altimetry data from Operation IceBridge are available at the National Snow and Ice Data Center (https://n5eil01u.ecs.nsidc.org/ICEBRIDGE/ILATM1B.001/ and https://n5eil01u.ecs.nsidc.org/ICEBRIDGE/ILATM1B.002/ for ATM, and https://n5eil01u.ecs.nsidc.org/ICEBRIDGE/ILVIS2.001/ for LVIS). Annual Antarctic ice velocity mosaics are available at https://n5eil01u.ecs.nsidc.org/MEASURES/NSIDC-0720.001/. The RACMO atmospheric variables and ice-shelf surface height time series from the IMAU Firn Densification Model used in this paper are available at ftp://ftp.esr.org/pub/datasets/AntPen/grl18/.

References

Arblaster, J. M., & Meehl, G. A. (2006). Contributions of external forcings to southern annular mode trends. *Journal of Climate*, *19*(12), 2896–2905. https://doi.org/10.1175/JCLI3774.1

Borstad, C., McGrath, D., & Pope, A. (2017). Fracture propagation and stability of ice shelves governed by ice shelf heterogeneity. *Geophysical Research Letters*, *44*, 4186–4194. https://doi.org/10.1002/2017GL072648

Borstad, C., Rignot, E., Mouginot, J., & Schodlok, M. (2013). Creep deformation and buttressing capacity of damaged ice shelves: Theory and application to Larsen C Ice Shelf. *The Cryosphere*, *7*(6), 1931–1947. https://doi.org/10.5194/tc-7-1931-2013

Cook, A. J., & Vaughan, D. G. (2010). Overview of areal changes of the ice shelves on the Antarctic Peninsula over the past 50 years. *The Cryosphere.*, *4*(1), 77–98. https://doi.org/10.5194/tc-4-77-2010

Dinniman, M. S., Klinck, J. M., & Hofmann, E. E. (2012). Sensitivity of Circumpolar Deep Water transport and ice shelf basal melt along the west Antarctic Peninsula to changes in the winds. *Journal of Climate*, *25*(14), 4799–4816. https://doi.org/10.1175/JCLI-D-11-00307.1

Dupont, T., & Alley, R. (2005). Assessment of the importance of ice-shelf buttressing to ice-sheet flow. *Geophysical Research Letters*, *32*, L04503. https://doi.org/10.1029/2004GL022024

Dutrieux, P., De Rydt, J., Jenkins, A., Holland, P. R., Ha, H. K., Lee, S. H., et al. (2014). Strong sensitivity of Pine Island ice-shelf melting to climatic variability. *Science*, *343*(6167), 174–178. https://doi.org/10.1126/science.1244341

Fricker, H. A., & Padman, L. (2012). Thirty years of elevation change on Antarctic Peninsula ice shelves from multimission satellite radar altimetry. *Journal of Geophysical Research*, *117*, C02026. https://doi.org/10.1029/2011JC007126

Hogg, A. E., Shepherd, A., Cornford, S. L., Briggs, K. H., Gourmelen, N., Graham, J. A., et al. (2017). Increased ice flow in Western Palmer Land linked to ocean melting. *Geophysical Research Letters*, *44*, 4159–4167. https://doi.org/10.1002/2016GL072110

Holland, P. R., Brisbourne, A., Corr, H. F. J., Daniel Mcgrath, K., Purdon, J., Paden, H. A., et al. (2015). Oceanic and atmospheric forcing of Larsen C Ice-Shelf thinning. *The Cryosphere*, *9*(3), 1005–1024. https://doi.org/10.5194/tc-9-1005-2015

Holland, P. R., Jenkins, A., & Holland, D. M. (2010). Ice and ocean processes in the Bellingshausen Sea, Antarctica. *Journal of Geophysical Research*, *115*, C05020. https://doi.org/10.1029/2008JC005219

Jenkins, A. (2011). Convection-driven melting near the grounding lines of ice shelves and tidewater glaciers. *Journal of Physical Oceanography*, *41*(12), 2279–2294. https://doi.org/10.1175/JPO-D-11-03.1

Jenkins, A., & Jacobs, S. (2008). Circulation and melting beneath George VI Ice Shelf, Antarctica. *Journal of Geophysical Research*, *113*, C04013. https://doi.org/10.1029/2007JC004449

Khazendar, A., Schodlok, M. P., Fenty, I., Ligtenberg, S. R. M., Rignot, E., & van den Broeke, M. R. (2013). Observed thinning of Totten Glacier is linked to coastal polynya variability. *Nature Communications*, *4*(2857), 1–9. https://doi.org/10.1038/ncomms3857

Kim, T., Ha, H., Wåhlin, A., Lee, S., Kim, C., Lee, J., & Cho, Y. (2017). Is Ekman pumping responsible for the seasonal variation of warm circumpolar deep water in the Amundsen Sea? *Continental Shelf Research*, *132*, 38–48. https://doi.org/10.1016/j.csr.2016.09.005

Kuipers Munneke, P., McGrath, D., Medley, B., Luckman, A., Bevan, S., Kulessa, B., et al. (2017). Observationally constrained surface mass balance of Larsen C Ice Shelf, Antarctica. *The Cryosphere*, *11*(6), 2411–2426. https://doi.rog10.5194/tc-11-2411-2017

Ligtenberg, S., Helsen, M., & Van den Broeke, M. (2011). An improved semi-empirical model for the densification of Antarctic firn. *The Cryosphere*, *5*(4), 809–819. https://doi.org/10.5194/tc-5-809-2011

Minchew, B. M., Gudmundsson, G. H., Gardner, A. S., Paolo, F. S., & Fricker, H. A. (2018). Modeling the dynamic response of outlet glaciers to observed ice-shelf thinning in the Bellingshausen Sea Sector, West Antarctica. *Journal of Glaciology*, 1–10. https://doi.org/10.1017/jog.2018.24

Morris, E. M., & Vaughan, D. G. (2003). Spatial and temporal variation of surface temperature on the Antarctic Peninsula and the limit of viability of ice shelves. *Antarctic Research Series*, *79*, 61–68. https://doi.org/10.1029/AR079p0061

Mouginot, J., Rignot, E., Scheuchl, B., & Millan, R. (2017). Comprehensive annual ice sheet velocity mapping using Landsat-8, Sentinel-1, and RADARSAT-2 data. *Remote Sensing*, *9*(4), 364. https://doi.org/10.3390/rs9040364

Mueller, R., Padman, L., Dinniman, M. S., Erofeeva, S., Fricker, H. A., & King, M. (2012). Impact of tide-topography interactions on basal melting of Larsen C Ice Shelf, Antarctica. *Journal of Geophysical Research*, *117*, C05005. https://doi.org/10.1029/2011JC007263

Mueller, R. D., Hattermann, T., Howard, S. L., & Padman, L. (2018). Tidal influences on a future evolution of the Filchner-Ronne Ice Shelf cavity in the Weddell Sea, Antarctica. *The Cryosphere*, *12*(2), 1–55. https://doi.org/10.5194/tc-2017-110

Nicholls, K., Pudsey, C., & Morris, P. (2004). Summertime water masses off the northern Larsen C Ice Shelf, Antarctica. *Geophysical Research Letters*, *31*, L09309. https://doi.org/10.1029/2004GL019924

Nilsson, J., Vallelonga, P., Simonsen, S. B., SÃÿrensen, L. S., Forsberg, R., Dahl-Jensen, D., et al. (2015). Greenland 2012 melt event effects on CryoSat-2 radar altimetry. *Geophysical Research Letters*, *42*, 3919–3926. https://doi.org/10.1002/2015GL063296

Padman, L., Costa, D. P., Dinniman, M. S., Fricker, H. A., Goebel, M. E., Huckstadt, L. A., et al. (2012). Oceanic controls on the mass balance of Wilkins Ice Shelf, Antarctica. *Journal of Geophysical Research*, *117*, C01010. https://doi.org/10.1029/2011JC007301

Padman, L., King, M., Goring, D., Corr, H., & Coleman, R. (2003). Ice-shelf elevation changes due to atmospheric pressure variations. *Journal of Glaciology*, *49*(167), 521–526. https://doi.org/10.3189/172756503781830386

Paolo, F. S., Fricker, H. A., & Padman, L. (2015). Volume loss from Antarctic ice shelves is accelerating. *Science*, *348*(6232), 327–331. https://doi.org/10.1126/science.aaa0940

Paolo, F. S., Fricker, H. A., & Padman, L. (2016). Constructing improved decadal records of Antarctic ice shelf height change from multiple satellite radar altimeters. *Remote Sensing of Environment*, *177*, 192–205. https://doi.org/10.1016/j.rse.2016.01.026

Paolo, F. S., Padman, L., Fricker, H. A., Adusumilli, S., Howard, S., & Siegfried, M. R. (2018). Response of Pacific-sector Antarctic ice shelves to the El Niño/Southern Oscillation. *Nature Geoscience*, *11*(2), 121–126. https://doi.org/10.1038/s41561-017-0033-0

Potter, J. R., & Paren, J. G. (1985). Interaction Between Ice Shelf and Ocean in George VI Sound, Antarctica. In S. S. Jacobs (Ed.), *Oceanology of the Antarctic Continental Shelf*. https://doi.org/10.1029/AR043p0035

Pritchard, H., Ligtenberg, S., Fricker, H., Vaughan, D., Van den Broeke, M., & Padman, L. (2012). Antarctic ice-sheet loss driven by basal melting of ice shelves. *Nature*, *484*(7395), 502–505. https://doi.org/10.1038/nature10968

Rignot, E., Casassa, G., Gogineni, P., Krabill, W., Rivera, A., & Thomas, R. (2004). Accelerated ice discharge from the Antarctic Peninsula following the collapse of Larsen B ice shelf. *Geophysical Research Letters*, *31*, L18401. https://doi.org/10.1029/2004GL020697

Scambos, T., Haran, T., Fahnestock, M., Painter, T., & Bohlander, J. (2007). MODIS-based Mosaic of Antarctica (MOA) data sets: Continent-wide surface morphology and snowgrain size. *Remote Sensing of Environment*, *111*(2-3), 242–257. https://doi.org/10.1016/j.rse.2006.12.020

Scambos, T. A., Bohlander, J., Shuman, C. U., & Skvarca, P. (2004). Glacier acceleration and thinning after ice shelf collapse in the Larsen B embayment, Antarctica. *Geophysical Research Letters*, *31*, L18402. https://doi.org/10.1029/2004GL020670

Scambos, T. A., Hulbe, C., Fahnestock, M., & Bohlander, J. (2000). The link between climate warming and break-up of ice shelves in the Antarctic Peninsula. *Journal of Glaciology*, *46*(154), 516–530. https://doi.org/10.3189/172756500781833043

Scambos, T., Hulbe, C., & Fahnestock, M. (2013). Climate-Induced Ice Shelf Disintegration in the Antarctic Peninsula. In E. Domack, et al. (Eds), *Antarctic Peninsula Climate Variability: Historical and Paleoenvironmental Perspectives*. Washington, DC: American Geophysical Union. https://doi.org/10.1029/AR079p0079

Schmidtko, S., Heywood, K. J., Thompson, A. F., & Aoki, S. (2014). Multidecadal warming of Antarctic waters. *Science*, *346*(6214), 1227–1231. https://doi.org/10.1126/science.1256117

Shepherd, A., Wingham, D., Payne, T., & Skvarca, P. (2003). Larsen ice shelf has progressively thinned. *Science*, *302*(5646), 856–859. https://doi.org/10.1126/science.1089768

Thomas, R., Davis, C., Frederick, E., Krabill, W., Li, Y., Manizade, S., & Martin, C. (2008). A comparison of Greenland ice-sheet volume changes derived from altimetry measurements. *Journal of Glaciology*, *54*(185), 203–212. https://doi.org/10.3189/002214308784886225

Thompson, D. W., & Solomon, S. (2002). Interpretation of recent Southern Hemisphere climate change. *Science*, *296*(5569), 895–899. https://doi.org/10.1126/science.1069270

Turner, J., Lu, H., White, I., King, J. C., Phillips, T., Hosking, J. S., et al. (2016). Absence of 21st century warming on Antarctic Peninsula consistent with natural variability. *Nature*, *535*(7612), 411–415. https://doi.org/10.1038/nature18645

van den Broeke, M. (2005). Strong surface melting preceded collapse of Antarctic Peninsula ice shelf. *Geophysical Research Letters*, *32*, L12815. https://doi.org/10.1029/2005GL023247

Van Wessem, J. M., Ligtenberg, S. R. M., Reijmer, C. H., van de Berg, W. J., van den Broeke, M. R., Barrand, N. E., et al. (2016). The modelled surface mass balance of the Antarctic Peninsula at 5.5 km horizontal resolution. *The Cryosphere*, *10*(1), 271–285.

Van Wessem, J. M., van de Berg, W. J., Noël, B. P. Y., van Meijgaard, E., Birnbaum, G., Jakobs, C. L., et al. (2017). Modelling the climate and surface mass balance of polar ice sheets using RACMO2. Part 2: Antarctica (1979–2016). *The Cryosphere Discussions*, 1–35. https://doi.org/10.5194/tc-2017-202

Wingham, D., Francis, C., Baker, S., Bouzinac, C., Brockley, D., Cullen, R., et al. (2006). CryoSat: A mission to determine the fluctuations in Earth's land and marine ice fields. *Advances in Space Research*, *37*(4), 841–871. https://doi.org/10.1016/j.asr.2005.07.027